MECOM99
Mendoza
6-10 de septiembre de 1999

FINITE ELEMENT SIMULATION OF HELICOPTER ROTOR IN HOVER

Norberto Nigro

Centro Internacional de Métodos Computacionales en Ingeniería
Instituto de Desarrollo Tecnológico para la Industria Química
Güemes 3450, C.P. 3000, Santa Fe, ARGENTINA
email: nnigro@intec.unl.edu.ar

ABSTRACT

This work deals with the application of a developed compressible Navier-Stokes finite element code to flow around helicopter's configurations. This is one of the first trials to apply this kind of numerical technique in this area where it is very common to find finite differences and finite volumes results. This study is part of a project that includes several stages of development covering from single rotor simulation in vertical and forward flight, interaction with fuselage, aeroelasticity, to the final goal which is the prediction of the aeroacoustic behaviour of the system and to diminish the noise generated by the coupling between fluid dynamic patterns. So, this problem contains a lot of interesting and challenging parts mostly under research. Here our concern is centered on the simulation of helicopter in hover condition including a preliminar study of the fluid dynamic phenomenon specially that concerned with blade vortex interaction in vertical flight. A video with the simulation results is presented.

INTRODUCTION

The need to accurately calculate the flowfield of an helicopter rotor in both hover and forward flight is of great practical importance. Unlike the flowfield of a fixed wing, the flowfield of an helicopter rotor is generally more complex to analyse because it provides some of the most complex challenges to be found in the field of applied aerodynamics. The complexity stem from several peculiar problems that are unique to the helicopter rotor. These include a radially increasing blade speed that is responsible for a high concentration of bound circulation over the outer portion of the blade, resulting in a strong trailed tip vortex and a spiraling wake vortex sheet. The vortical wake initially remains close to the rotor, causing strong blade-vortex interactions. Other factors are the high centrifugal force field in which the blades operate, the relatively large steady-state out-of-plane displacement of the rotor blades and aeroelastic response of the rotor itself and finally, mutual interaction of flowfields of main rotor, tail rotor and the fuselage. These flowfield are often characterized by transonic conditions and associated shock waves, which make the flow susceptible of threedimensionality and unsteadiness.[1] The operating characteristics of such rotary-wing vehicles are strongly influenced by the vortex wake. The interaction of this wake with the following blades is a potential source of noise and vibration at low and moderate flight speeds. Discrete frequency noise is usually divided into deterministic components of thickness and loading noise, blade-vortex interaction noise and high speed impulsive noise. On the other hand we have the broadband noise consisting of the non-deterministic loading noise sources of turbulence noise, blade-wake interaction noise and blade self noise.[2] Accurate prediction of the vortical wake

is probably the most important, most studied and the most difficult aspect of helicopter flowfield. Current methods of analysis of the wake range in complexity from relatively simple momentum theory applications to free wake lifting surface methods. The inadequacies of these methods have led to recent efforts to use state of the art computational fluid dynamics (*CFD*) codes to shed more light on the understanding of this problem. Finite difference codes for nonlinear compressible potential equations[3,4] and Euler equations[5,6,7,8,9] have been used to calculate the rotor flowfield. Initially developed methods using the potential flow and the Euler formulations were primarily limited to calculating nonlifting rotor flow because of the inherent limitation of being unable to model the vortex wake with these equations, altough the Euler formulation has in it the neccesary physics to model vorticity transport correctly. These equations basically lack the physical mechanism needed to generate the vortex wake. However, in conjunction with wake models supplied by other specific codes both potential and Euler codes have been extensively used to calculate the lifting rotor flowfields. The standard experimental data that is used in validating most of these codes has been the two bladed rotor data of Caradonna and Tung.[10] An excellent review of some of the currently available inviscid finite difference numerical methods have also been presented by Caradonna and Tung[11] One of the most important part of the helicopter rotor flowfield is that represented by tip vortices. This vortices located at the tips of the rotating blades along with helical wake vortex sheet have tremendous influence on the operating characteristics of the rotor. Some of the common practical problems caused by such concentrated trailing vortices are the rotor vibration due to unsteady lift fluctuations, increased induced drag and the annoying "blade-slap" (an impulsive noise characteristic). Most of the studies carried out are basically inviscid in nature and therefore preclude the physical mechanisms neccesary to model correctly the formation of the tip vortex which involves the complex three dimensional viscous flowfield in the tip region. Just after the supercomputers were available it was possible to apply Navier-Stokes simulations to this kind of flows. Understanding the mechanism of the tip vortex formation and its subsequent rollup would provide a proper insight to control these tip flows and alleviate some of the problems caused by them. The ability to preserve the concentrated vortices in the finite-difference grid without numerical diffusion has been the biggest setback until now for progress in this area. Even the most advanced computational techniques, which use spatial central differencing, lack then proper mechanism to preserve concentrated tip vortices and convect them in the flowfield without numerical diffusion. However the recently developed upwind schemes in conjunction with a proper grid choice appear very promising to preserve and convect concentrated vortices. Alternatively if the properly captured tip vortex is analytically represented then prescribed vortex methods could be applied to calculate the vortex wake development for several rotations of the blade. These methods have demonstrated the ability to preserve and convect concentrated vortices even in very coarse grid regions without significant numerical diffusion.[1] The first part of this project consists of the application of a developed finite element compressible Navier-Stokes code for hovering helicopter rotor and general vertical flight using different geometries, starting only with the rotor and then including different fuselage selections. In the author knowledge there is not a previous paper dealing with the use of finite element in helicopter rotor simulation. The simple geometry involved in the first simulations allow to take periodical boundary conditions around the rotation axis and therefore the computational domain only cover $\frac{2\pi}{N}$, where N is the number of blades. In order to validate our code we will begin with flow around an helicopter rotor without fuselage. For this example there are several results using potential, inviscid and viscous finite volumes codes and we can use them as a pattern of comparison. In the next sections we present the compressible Navier-Stokes equations, the finite element formulation used as spatial discretization, some topics related with GMRES implicit solver and some important remarks about the boundary condition treatment. Finally we show a video with the results of two numerical simulations, the first for subsonic tip Mach number and the last for a critical value.

PROBLEM STATEMENT

In this section we include several aspects related with the numerical simulation of fluid flow around

helicopter configuration in hover.

The problem is established in a non-inertial frame to treat the centrifugal and Coriolis forces[12] and for this first stage of the project we focus on the steady state solution. The physics involved in our fluid dynamic problems is mathematically governed by Navier-Stokes equations. 3D Compressible Navier-Stokes equations are classically written in terms of *conservative variables* in the following form:

$$\mathbf{F}^i_{a,i} = \mathbf{F}^i_{d,i} + \mathcal{F} \ , \tag{1}$$

Implicitly we assume $(\ )_{,i} = \partial(\ )/\partial x_i$.

$\mathbf{U} \in \mathbb{R}^5$ is the fluid local state vector, where $\mathbf{U} = [\rho, \rho\mathbf{u}^T, \rho e]^T$, with $\rho, \mathbf{u}, e$ as the density, velocity and total energy of the fluid. $\mathbf{F}_a, \mathbf{F}_d \in \mathbb{R}^{5\times 3}$ are the advective and diffusive fluxes, respectively, that depend on the state vector and its gradient as:

$$\mathbf{F}_a(\mathbf{U}) = \begin{bmatrix} \rho\mathbf{u}^T \\ \rho\mathbf{u}\mathbf{u}^T + p\mathbf{I}_{3\times 3} \\ (\rho e + p)\mathbf{u}^T \end{bmatrix} \qquad \mathbf{F}_d(\mathbf{U}, \nabla\mathbf{U}) = \begin{bmatrix} 0 \\ \sigma \\ (\sigma\cdot\mathbf{u} + \mathbf{q})^T \end{bmatrix} \tag{2}$$

where $p, \sigma, \mathbf{q}$ are the thermodynamic pressure, the stress deviatoric tensor and the heat flux vector, respectively, with

$$\begin{aligned} \sigma_{jk} &= \mu(u_{j,k} + u_{k,j}) + \lambda u_{l,l}\delta_{jk} \\ q_j &= \kappa\theta_{,j} \end{aligned} \tag{3}$$

where μ is the effective dynamic viscosity (considering the turbulence viscosity coming from Baldwin-Lomax model[13]), λ is the second viscosity coefficient, κ the thermal conductivity and θ the temperature.

We finish the description of the mathematical model, introducing the state equation of the fluid and the relation between the energy and two of the thermodynamic variables of the fluid. Specifically we use the ideal gas law

$$\begin{aligned} p/\rho = R\theta = C_v(\gamma-1)\theta = (\gamma-1)e \\ p = (\gamma-1)\rho i \end{aligned} \tag{4}$$

where R and C_v represent the gas universal constant and the specific heat at constant volume respectively and i is the internal energy

$$i = e - \frac{1}{2}||\mathbf{u}||^2 \tag{5}$$

The body force $\mathcal{F}$ is:

$$\mathcal{F} = \rho \begin{pmatrix} 0 \\ \mathrm{f}_{\mathrm{Cor}} + \mathrm{f}_{\mathrm{Cent}} \\ \mathrm{f}_{\mathrm{Cent}} \cdot \mathbf{u} \end{pmatrix} \tag{6}$$

being $\mathrm{f}_{\mathrm{Cor}} = -2\boldsymbol{\Omega} \times \mathbf{u}$ and $\mathrm{f}_{\mathrm{Cent}} = -\boldsymbol{\Omega} \times \boldsymbol{\Omega} \times \mathbf{x}$ the Coriolis and centrifugal force, respectively. This kind of advective-diffusive system is incompletely parabolic and not completely parabolic because the continuity equation has not diffusive term. In the Euler equations case we can use the above system dropping the diffusive flux terms $\mathbf{F}_d^i$, resulting in a pure advective hyperbolic system.

It is useful to rewrite the equation 1 in a quasi-linear form

$$\mathbf{A}_j \mathbf{U}_{,j} = (\mathbf{K}_{ij} \mathbf{U}_{,j})_{,i} + \mathcal{F} \tag{7}$$

where $\mathbf{A}_j = \partial \mathbf{F}_a^j / \partial \mathbf{U}$ is the jth advective jacobian matrix and $\mathbf{K}_{ij}$ is one of the components of the whole tensor $\mathbf{K}$ that represent the diffusive jacobian matrix, with $\mathbf{F}_d^i = \mathbf{K}_{ij} \mathbf{U}_{,j}$. Expressions for the above jacobian matrices may be found in several references,[14,15,16,17].

SPATIAL DISCRETIZATION BY FEM

In order to get a numerical solution of the continuum problem presented in the first section we have to discretize the problem using a particular numerical method. In this work we use an SUPG technique that is very popular in the context of Finite Element Method and is one of the most referenced in the CFD area,[14,18,19,20,21,22,23,24,15,16,25,26,17] It is based on Petrov-Galerkin weighted residual method which allows to use test functions that can be different from the interpolation ones and not necessarily continuous. This method introduces the numerical dissipation needed to stabilize the system in advection-dominated problems, keeping the consistency with the continuum problem. For each node a there is an interpolation function $\mathbf{N}_a$ (hat type in $1D$, bilinear in $2D$, and multilinear in general) and a test function $\mathbf{W}_a = \mathbf{N}_a + \mathbf{P}_a$, where $\mathbf{P}_a$ is called the perturbation function. The standard Galerkin method is recovered when we impose $\mathbf{P}_a \equiv 0$. The $\mathbf{W}_a$ (and, of course, $\mathbf{P}_a$) are not necessarily continuous through the inter-element boundaries. The variational formulation of the problem is written in the following form: Given a finite element partition

of the original domain Ω into elements Ω_e , $e = 1, \ldots, N_{el}$ with N_{el} the number of elements in the mesh.

Then the problem is finding $\mathbf{U}^h \in \mathcal{S}$ such that $\forall\ \mathbf{N} \in \mathcal{V}$

$$\int_\Omega \left(\mathbf{N}_a^T \mathbf{A}_i \mathbf{U}_{,i}^h + \mathbf{N}_{a,i}^T \mathbf{K}_{ij} \mathbf{U}_{,j}^h \right) \, d\Omega + \\ + \sum_{e=1}^{N_{el}} \int_{\Omega_e} \mathbf{P}_a^{eT} \left(\mathbf{A}_i \mathbf{U}_{,i}^h - (\mathbf{K}_{ij} \mathbf{U}_{,j}^h)_{,i} - \mathcal{F} \right) \, d\Omega = \int_\Omega \mathbf{N}_a^T \mathcal{F} + \int_{\Gamma_h} \mathbf{N}_a^T \mathbf{h} \, d\Gamma \tag{8}$$

is satisfied, where $\mathbf{h}$ is the diffusive flux imposed on the boundary Γ_h and $\mathbf{U}^h$ is the finite element approximation of $\mathbf{U}$. $\mathcal{S}$ and $\mathcal{V}$ are the trial and weighting function spaces respectively, commonly used in this context.[14,16]

The Euler-Lagrange form is obtained through classical integration by parts:

$$\sum_{e=1}^{N_{el}} \int_{\Omega_e} \mathbf{W}_a^T \left(\mathbf{A}_i \mathbf{U}_{,i}^h - \mathbf{K}_{ij} \mathbf{U}_{,ij}^h - \mathcal{F} \right) \, d\Omega + \int_{\Gamma_{int}} \mathbf{N}_a^T \left[n_i \mathbf{K}_{ij} \mathbf{U}_{,j}^h \right] \, d\Gamma + \int_{\Gamma_h} \mathbf{N}_a^T \left(n_i \mathbf{K}_{ij} \mathbf{U}_{,j}^h - \mathbf{h} \right) \, d\Gamma = 0 \tag{9}$$

$$\text{where:} \qquad \left[n_i \mathbf{K}_{ij} \mathbf{U}_{,j}^h \right] (\mathbf{x}) = n_i(\mathbf{x}) \left\{ (\mathbf{K}_{ij} \mathbf{U}_{,j}^h)(\mathbf{x}^+) - (\mathbf{K}_{ij} \mathbf{U}_{,j}^h)(\mathbf{x}^-) \right\} \tag{10}$$

is the jump in the diffusive flux throughout the inter-element boundary, $\mathbf{x}$ is a point which lies there, $\mathbf{x}^{\pm}$ are points belonging to each side of the boundary and Γ_{int} is the inter-element contour. Consistency is warranted because the continuum solution is also solution of this variational formulation. As we mentioned earlier the goal in SUPG scheme relies on the modification of the standard basis functions in order to stabilize the discretized problem. Since the publication of the original work in 1982 by Brooks and Hughes[20] a lot of work was developed around this subject and a complete list of contributions is out of the scope of this work. It is important to mention that several different perturbation function approaches have arisen since the original paper. Here we adopt that most commonly used for Euler and Navier-Stokes equations,[22 15 26 17] i.e.

$$\mathbf{P}_a^e = \tau^T \mathbf{A}_i^T \mathbf{N}_{,i} \tag{11}$$

In this expression appears a matrix τ that varies from different authors and represents the critical point of the design of the stabilization method. Sometimes called *"intrinsic time scale matrix"*, it can be deduced through its application to simple situations where an exact analytical solution is possible to find. Its generalization is so difficult and relays on heuristic arguments. In this code we have used the following definition for this matrix:

$$\tau = ||\mathbf{B}||^{-1} = (|\mathbf{B}_1| + |\mathbf{B}_2| + |\mathbf{B}_3|)^{-1} \tag{12}$$

with $|\mathbf{B}_i| = \mathbf{S}_i^{-1} |\mathbf{\Lambda}_i| \mathbf{S}_i$, $\mathbf{S}$ and $\mathbf{\Lambda}$ are the corresponding eigenvector and eigenvalue matrices.[27]

This expression is valid only for inviscid flows (Euler equations), or it is equivalent to a full upwind scheme for viscous flows introducing too much diffusion. In this work we have extended the above definition to Navier-Stokes equations using an scalar factor that is proportional to the Reynolds and Prandtl numbers and was introduced by Soulaimani et.al .[25]

IMPLICIT ITERATIVE SOLVER

As we are interested in steady state solutions, the transient term in the right hand side is neglected and including the time discretization by a finite differences scheme we finally reach the following system:

$$\left(\frac{1}{\Delta t} \mathbf{M} + \mathbf{C}(\mathbf{U}) \right) \Delta \mathbf{U} = \mathbf{R}(\mathbf{U}), \tag{13}$$

where $\mathbf{M}, \mathbf{C} = \mathbf{R}_{,\mathbf{U}}$ and $\mathbf{R}$ represent the mass matrix associated with the discretization of temporal terms, the residual jacobian matrix and the residual vector, respectively. The computation of steady solutions using time marching algorithm allow us to select the time step according to temporal stability and convergence rate criteria. In the case of explicit solver we know that exists a critical time step that is function of several

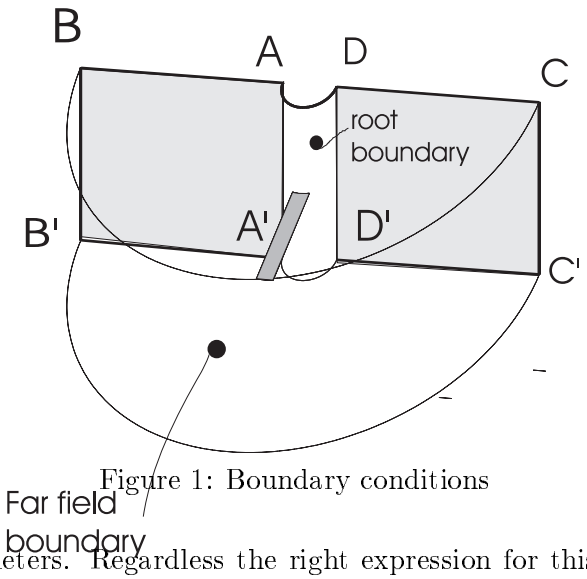

Figure 1: Boundary conditions

numerical and physical parameters. Regardless the right expression for this critical time step[16] we know that one of the principal factor that influence on its determination is the element size. If we adopt a global time step (the same for all the elements) we penalize those elements which big size. While accuracy in time were not our concern we can adopt a very popular strategy called *time local stepping*[28] in which each element of the mesh has its own time step in order to improve the rate of convergence. As it is usual the criterion is to equalize the Courant number for all the elements. This strategy is specially needed when there is a strong refinement in the mesh due to the physical properties of the flow involved in the computation, like shocks, boundary layers among others. Even though this strategy is specially adapted to explicit computations its implementation within an implicit solver produce some interesting improvement of the convergence rate.[14] The solution of the linear algebraic system 13 may be accomplished by different strategies. In the *explicit* case $\tilde{\mathbf{M}}$ is usually lumped in order to get a diagonal matrix. Then the solution of the linear system decouples and it is no neccesary neither to invert nor to store any matrix. These advantages and its own simplicity make the explicit solver one of the most popular ways to solve linear systems. Its disadvantage is associated with the strong limitations imposed by stability criteria. In the general *implicit* case we need to store and invert the left side matrix and for this task we can choose among direct or iterative solvers. Direct solvers are frequently used in small and medium size computations like those that appear in 2D problems but its generalization to 3D problems is restricted for memory and CPU time resources. In this case we are constrained to use iterative methods. In this work we have used a matrix-free GMRES , one of the most referenced iterative solvers in CFD applications during the last years[2930] To accelerate the convergence of the GMRES algorithm we have used two different kind of preconditioners. The first one is introduced into the temporal term like a mass matrix affecting the time evolution of the solution keeping the same steady solution. This matrix, called $\mathbf{\Gamma}$[31] improves the convergence rate for all Reynolds and Mach numbers modifying the characteristic speeds without altering the physical sense of the problem. The details about this preconditioner are out of the scope of this paper. For further references, see[32].[31] The second preconditioner plays the role of an scaling for the GMRES method and in this work we have used a right preconditioner based on nodal block diagonal matrix[32][14].[16] To circumvent memory resources restriction in large 3D computation we have used a matrix-free version of this algorithm.[14]

BOUNDARY CONDITIONS

Figure 1 shows the computational domain and the boundary conditions specified for our simulations.

• **Blade root boundary conditions** This boundary is generated by a cylinder of radius R_1 that surround the rotation axis. It is represented by the surface AA'D'D in figure 1. In this boundary we have applied symmetry boundary conditions,

$$\text{symmetry b.c.} \quad \Rightarrow \begin{cases} u_n = 0 \\ \tau_{rn} = 0 \\ \tau_{sn} = 0 \\ \theta_{,n} = 0 \end{cases} \tag{14}$$

where (r, s, n) are the coordinate axes of a local frame.

• **Profile boundary conditions**

$$\begin{cases} u = v = w = 0 \\ \theta = \theta_w \end{cases} \tag{15}$$

with θ_w the temperature of the profile.

• **Periodic boundary conditions** Represented by two planes where exist scalar and vector periodicity of the variables involved in the computation. In figure 1 the planes AA'B'B and DD'C'C were considered periodic. In these planes we assume that scalar variables are the same and vectorial variables like velocity vector are the sames unless the respective rotation between the two planes.

• **Far-field boundary conditions** The planes ABCD , A'B'C'D' and BB'C'C are far-field boundaries. (see figure 1) For this boundary we may apply several strategies. The first one could be standard *Dirichlet* boundary conditions with special care about which variable should be fixed. A general rule for compressible flow takes account of the Mach number and the normal vector of the boundary in order to determine the variables to be fixed. The second strategy that is very popular for far field boundaries is known as *absorbent* boundary conditions. To apply them we transform the differential operator at the boundary and we recover the characteristics variables. Then we fix those characteristics variable which enter to the domain to a reference set of variables and we extrapolate the interior variables for those characteristics which leave the domain. Finally, the third strategy is specially designed for hover helicopter rotors. This kind of treatment arose because the inadecuacies of the standard boundary conditions for this application. Briefly, we can explain the difficulties through the recirculating box created by the computational domain when the rotor is spinning. The quiescent flow conditions at far-field boundary enforce this situation in order not to violate the conservation laws. The real situation is that the rotor enforce a mass flow that depends on the rotation of the blade and is entering to the domain in some parts and exiting in another ones. For a more realistic model a three-dimensional point sink in conjunction with a 1D momentum theory[33] was presented by Srinivasan et-al.[34] To describe this model we need to compute two velocities,

$$W_{\text{in}} = -\frac{M_{\text{tip}}}{4}\sqrt{\frac{C_T}{2}}\left(\frac{R}{d}\right)^2 \tag{16}$$

that generated by the point sink model and it is evident that is proportional to the radial distance to the center of rotation (d), regardless the particular coordinate of the point. In this expression R is the radial distance relative to the coordinate origin and M_{tip} is the Mach number at the tip of the blade.

The second one is called the exit velocity and appears from a simple momentum theory as:

$$W_e = -M_{\text{tip}}\sqrt{\frac{C_T}{2}} \tag{17}$$

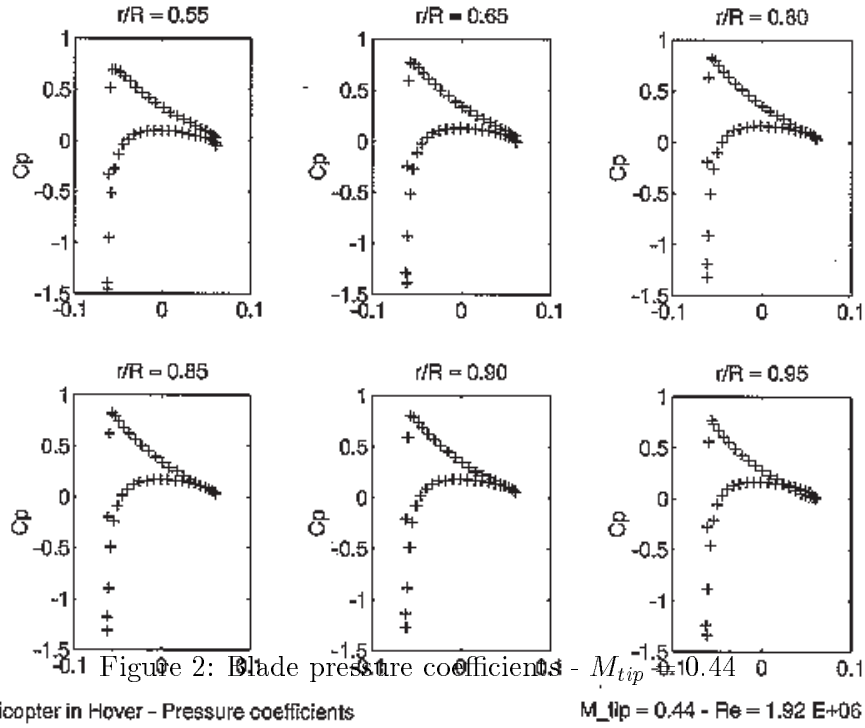

Figure 2: Blade pressure coefficients - $M_{tip} = 0.44$

In both expressions appears the rotor thrust coefficient C_T that depends on the rotational dynamic pressure q_{tip} being T the thrust.

$$\begin{aligned} C_T &= \frac{T}{2\pi R^2 q_{\text{tip}}} \\ q_{\text{tip}} &= \frac{1}{2}\rho(\Omega R)^2 \end{aligned} \tag{18}$$

NUMERICAL RESULTS

The test cases were extracted from some numerical simulations and the popular experimental data set of Caradonna and Tung[10].[11] It consists of a two-bladed rigid rotor with rectangular planform blades with no twist or taper. The blades are made of NACA 0012 airfoil sections with an aspect ratio of 6. Two experimental situations were tested, one for a subsonic tip speed an the last for a transonic case, both with the same collective pitch angle of $\theta_c = 8°$. Reynolds number, based on the blade tip speed and the chord of the blade was $Re = 1.92 \times 10^6$ and Re $= 3.93 \times 10^6$ respectively. Both numerical experiments demanded approximately four CPU hours to reach a reasonable convergence level.

Mesh generation. The ad-hoc grid generator consists of an structured mesh generator that builds a 3D mesh by extrusion of a 2D grid. We divide the whole domain in several zones in a similar fashion like a multiblock grid generator. The first zone is basically composed by the blade and its vicinity. This region contains the blades itself and is generated by taking a radial projection of the mesh and shifting in the radial direction from the inner radius to the outer one. For each radial station we have used an O mesh around a

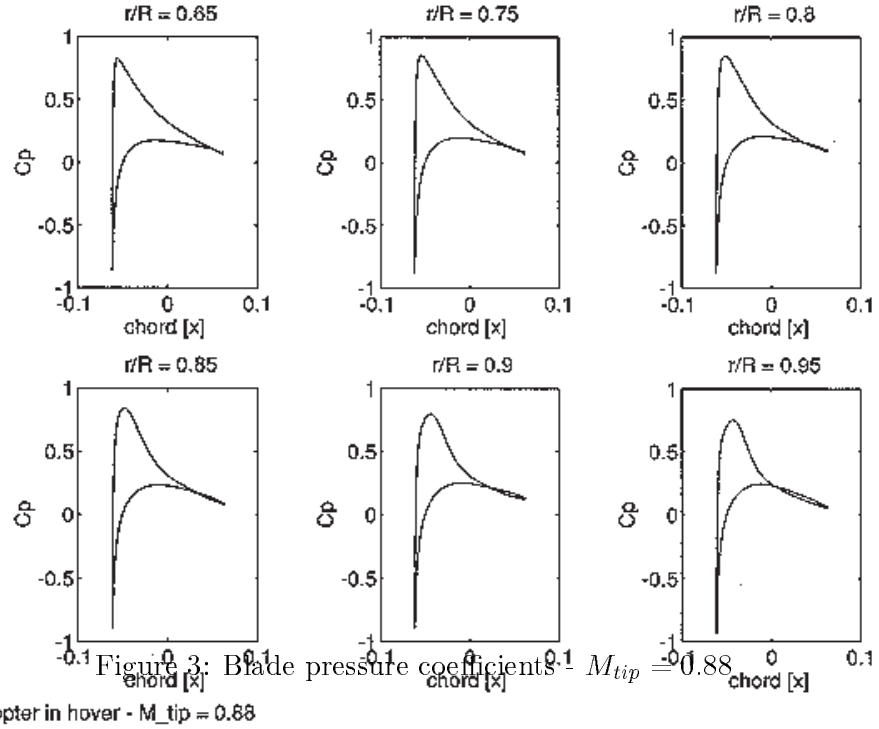

Figure 3: Blade pressure coefficients - $M_{tip} = 0.88$

given NACA 12 profile. It is possible to specify any type of profiles in this stage. In the present work we adopt an untappered blade tip. It is remarkable that this part of the mesh is refined due to the presence of the vortex tip. We fill the far field domain around the blade with an structured mesh. The mesh contains around 50,000 hexahedral elements.

$M_{\mathbf{tip}} = 0.44$ Figure 2 shows the pressure coefficient for six radial stations covering from $r/R = 0.55$ to $r/R = 0.95$. The tip Mach number is subsonic, around 0.44. These results are in good agreement with those reported in several references,[10],[11],[1],[34]

$M_{\mathbf{tip}} = 0.88$ In this case a shock wave pattern with a high suction region over the blade is obtained by the algorithm. Figure 3 shows the pressure coefficient for several radial stations for the transonic tip case giving again a good agreement with other numerical and experimental results,[10],[11],[1],[34]

A video with several frames showing streamlines from diferent point of view is included where it is possible to visualize not only the helical vortex sheet shape also the presence of a separation region close to the tip and the corresponding reattachment.

CONCLUSIONS

The flowfield of a hovering rotor was computed by a finite element code with an efficient implicit solver for the solution of compressible Navier-Stokes equations. To simplify the mesh generation procedure we have adopted a multiblock grid strategy with structured blocks inside each block. A very effective set of boundary conditions was applied in order to capture some important effects related with the formation of

vortices and wakes. Two different examples were performed and the preliminar numerical predictions are relatively good considering that the mesh used was relatively coarse (approximately 50,000 elements).

ACKNOWLEDGEMENT

The author wish to express their gratitude to *Consejo Nacional de Investigaciones Científicas y Técnicas* (CONICET, Argentina) for its financial support and to Tayfun Tezduyar for his guidance in this research. Cray C90 time was provided by the University of Minnesota Supercomputer Institute.

References

[1] G. Srinivasan, W. McCroskey. Navier-Stokes calculations of hovering rotor flowfields. *Journal of Aircraft*, 25(10), 1988.

[2] K. Brentner, F. Farassat. Helicopter noise predictions: The current status and future direction. *Journal of Sound and Vibration*, 170(1), 1994.

[3] R. Strawn, F. Caradonna. Conservative full potential model for unsteady transonic rotor flows. *AIAA Journal*, 25(2), 1987.

[4] T. Egolf, S. Sparks. Hovering rotor airload prediction using a full potential flow analysis with realistic wake geometry . In *42nd Annual Forum of the American Helicopter Society*. American Helicopter Society, Washington DC., 1986.

[5] R. Agarwal, J. Deese. Euler calculations for flowfield of a helicopter rotor in hover. *Journal of Aircraft*, 24(4), 1987.

[6] C. Chen, W. McCroskey. Numerical simulation of helicopter multi-bladed rotor flow. *AIAA paper*, 88-0046, 1988.

[7] I. Chang, C. Tung. Euler solution of the transonic flow for a helicopter rotor. *AIAA paper*, 87-0523, 1987.

[8] T. Roberts, E. Murman. Solution method for a hovering helicopter rotor using the Euler equations. *AIAA paper*, 85-0436, 1985.

[9] B. Wake, N. Sankar, S. Lekoudis. Computation of rotor blade flows using the Euler equation. *Journal of Aircraft*, 23(7), 1986.

[10] F. Caradonna, C. Tung. Experimental and analytical studies of a model helicopter rotor in hover. Technical Report TM-81232, NASA, USA, February 1981.

[11] F. Caradonna, C. Tung. A review of current finite differences rotor flow codes. In *42nd Annual Forum of the American Helicopter Society*. American Helicopter Society, Washington D.C., 1986.

[12] N. Nigro, M. Storti, S. Idelsohn. Fluid flows around turbomachinery using an explicit pseudo-temporal Euler FEM. *Communications in Applied Numerical Methods*, 11, 1995.

[13] B. Baldwin, H. Lomax. Thin layer approximation and algebraic model for separated turbulent flow. *AIAA Paper*, 78-257, 1978.

[14] S. Aliabadi. *Parallel finite element computations in aerospace applications.* PhD thesis, Department of Aerospace Engineering and Mechanics, University of Minnesota, Minneapolis, USA, 1994.

[15] M. Mallet. *A finite element method for CFD .* PhD thesis, Department of Civil Engineering, Stanford University, California, USA, 1985.

[16] F. Shakib. *Finite element analysis of the compressible Euler and Navier-Stokes equations.* PhD thesis, Department of Civil Engineering, Stanford University, California, USA, 1988.

[17] T.J.R. Hughes, T. Tezduyar. Finite Element methods for fisrt-order hyperbolic systems with particular emphasis on the compressible Euler equations. *Comp. Meth. in Applied Mechanics and Engineering*, 45, 1984.

[18] S. Aliabadi, S. Ray, T. Tezduyar. SUPG finite element computation of viscous compressible flows based on the conservation and entropy variables formulations. *Computational Mechanics*, 11, 1993.

[19] C. Baumann, M. Storti , S. Idelsohn. A Petrov-Galerkin Technique for the solution of transonic and supersonic flows. *Comp. Meth. in Applied Mechanics and Engineering*, 95, 1992.

[20] A. Brooks, T.J.R. Hughes. Streamline Upwind/Petrov-Galerkin Formulations for Convection Dominated Flows with Particular Emphasis on the Incompressible Navier-Stokes Equations. *Comp. Meth. Applied Mechanics and Engineering*, 32, 1982.

[21] T.J.R. Hughes, M. Mallet, A. Mizukami. A new finite element method for CFD: II. Beyond SUPG. *Comp. Meth. in Applied Mechanics and Engineering*, 54, 1986.

[22] T.J.R. Hughes, M. Mallet. A new finite element method for CFD: III. The generalized streamline operator for multidimensional advection-diffusion systems. *Comp. Meth. in Applied Mechanics and Engineering*, 58, 1986.

[23] T.J.R. Hughes, M. Mallet. A new finite element method for CFD: IV. A discontinuity-capturing operator for multidimensional advective-diffusive systems. *Comp. Meth. in Applied Mechanics and Engineering*, 58, 1986.

[24] G. Le Beau, S. Ray, S. Aliabadi, T. Tezduyar. SUPG finite element computation of compressible flows with the entropy and conservation variables formulations. Submitted to Comp. Meth. in Applied Mechanics and Engineering, 1993.

[25] A. Soulaimani, M. Fortin. Finite element solution of compressible viscous flows using conservative variables. *Comp. Meth. in Applied Mechanics and Engineering*, 118, 1994.

[26] T. Tezduyar, T.J.R. Hughes. Finite Element formulations for convection dominated flows with particular emphasis on the compressible Euler equations. *AIAA Paper*, 83-0125, 1983.

[27] M. Storti, N. Nigro, S. Idelsohn. Steady state incompressible flows using explicit schemes with an optimal local preconditioning. *Comp. Meth. in Applied Mechanics and Engineering*, 124, 1995.

[28] B. van Leer, W. Lee, P. Roe. Characteristic time-stepping or local preconditioning of the Euler equations. *AIAA Paper*, 91-1552-CP, 1991.

[29] Y. Saad . A flexible inner-outer preconditioned GMRES algorithm. *SIAM Journal on Scientific Computing*, 14, 1993.

[30] Y. Saad, M. Schultz . GMRES: A generalized minimal residual algorithm for solving nonsymmetric linear systems. *SIAM Journal on Scientific and Statistical Computing*, 7, 1986.

[31] Y. Choi, C. Merkle. The application of preconditioning in viscous flows. *Journal of Computational Physics*, 105, 1993.

[32] N. Nigro, M. Storti, S. Idelsohn, T. Tezduyar. Physics based GMRES preconditioner for compressible and incompressible Navier-Stokes equations. *Comp. Meth. in Applied Mechanics and Engineering*, 154, 1998.

[33] W. Stepniewski, C. Keys. *Rotary-wing aerodynamics*. Dover Publications, New York., 1984.

[34] G. Srinivasan, V. Raghavan, E. Duque, W. McCroskey. Flowfield analysis of modern helicopter rotors in hiver by Navier-Stokes method. *Journal of the American helicopter society*, 38(3), 1993.